Fatigue Crack Growth Analysis using TSA

F.A. Diaz, E.A. Patterson and J.R. Yates

The University of Sheffield, Department of Mechanical Engineering, Mappin Street, S1 3JD, Sheffield, U.K., E-mail: f.a.diaz@sheffield.ac.uk

ABSTRACT. *Modern experimental techniques provide valuable information for understanding fatigue phenomena such as crack closure and crack paths in complex stress fields. Thermoelastic Stress Analysis is a non-contact technique that provides full-field stress maps from the surface of structural components by measuring the small temperature changes at the surface of the structure arising from cyclic loading. The technique appears to have great potential in the study of crack closure since the crack tip stresses are inferred from the temperature changes that occur in the component. This means that the effective stress intensity factor range of the growing crack can be evaluated directly from the experimental data. The preferred method of analysis to derive stress intensity factors is based on Muskhelishvili's complex potentials. A new approach has been developed that not only makes it possible to calculate the mode I and mode II stress intensity factors but also to locate the crack tip and, consequently, to monitor the fatigue crack path.*

In this paper is a description of the fundamentals of the thermoelastic stress analysis technique and a summary of the different approaches to the experimental evaluation of the SIF. A description of the new methodology for the mathematical analysis of thermoelastic images for the location of the crack tip is presented. The application of the latest TSA developments to two important structural integrity problems is presented and discussed. The first is the evaluation of the effect of residual stresses on the closure of a fatigue crack growing through a weld. The second is the automatic tracking of a fatigue crack growing from a starter defect. The advances made in dealing with both these issues means that TSA likely to become an even more important tool in structural integrity research.

INTRODUCTION

The ability to make reliable measurements of the stresses around a crack tip is an essential part of understanding the nature of the fatigue process. Both analytical models and numerical simulations are dependent on good quality experimental data if they are to provide useful information for engineers and scientists.

Experimental strain analysis techniques such as strain gauging, photoelasticity, moiré interferometry and theremoelasticity all have a place in the tool kit of the experimentalist. Recent developments in infrared camera technology and new ideas on processing the data mean that thermoelastic stress analysis offers some particular advantages to those involved in research into fatigue crack propagation.

This paper starts with a description of the fundamentals of the thermoelastic technique and the different approaches used for the experimental evaluation of stress intensity factors from thermoelastic data. A description of a new methodology for the mathematical analysis of thermoelastic images for the location of the crack tip is also given. The technique was used to study the growth of a fatigue crack in a ferritic steel weld. The equipment used for testing and the experimental work conducted is described. Finally, some results showing that the crack path could be located and the effective stress intensity factor of the growing crack could be determined.

OVERVIEW OF EXPERIMENTAL APPROACHES TO FRACTURE MECHANICS

The accurate determination of the stress intensity factor of a crack in an engineering component is not a straightforward process. In fatigue tests on specimens of simple geometry it is not uncommon to use the compliance method, in which a remote measurement of strain is used to monitor the change in specimen compliance from which the stress intensity factor is deduced. This approach is not readily applicable to a more complex geometry, and optical techniques based on a field of data from around the crack provide a valuable alternative.

Many methods of evaluating the stress intensity factor from measurements of the strain field around the crack tip have developed over the years. There is essentially at least one method to accompany each technique of experimental stress analysis. Each technique has its champions who have developed, refined and validated the methods by comparison to analytical and, or numerical results. The choice available to the engineer or scientist who requires a means of measuring the stress intensity factor is large and there are few works in the open literature to help make the decision on which technique to use in a particular situation. Two that do exist are by Sanford [1], who provided a useful overview of the full-field optical techniques, and by Patterson and Olden [2], who conducted a study to make direct comparisons between competing optical strain analysis techniques.

Principles of Determining Fracture Mechanics Parameters from Experimental Data

The stress field around a crack tip can be described by the set of linear elastic field equations [3] in which the stress intensity factors K_I, $K_{II,}$ and K_{III} are parameters that characterise the field. The evaluation of the stress intensity factors from experimental data involves solving these equations using measurements to provide boundary conditions. The most commonly used form of the stress field equations can be derived using Westergaard's [4] approach and by making a first order approximation gives:

$$\sigma_x = \frac{K_I}{\sqrt{2\pi r}}\cos\frac{\theta}{2}\left(1-\sin\frac{\theta}{2}\sin\frac{3\theta}{2}\right)+\sigma_{ox}$$
$$\sigma_y = \frac{K_I}{\sqrt{2\pi r}}\cos\frac{\theta}{2}\left(1+\sin\frac{\theta}{2}\sin\frac{3\theta}{2}\right) \quad (1)$$
$$\tau_{xy} = \frac{K_I}{\sqrt{2\pi r}}\sin\frac{\theta}{2}\cos\frac{\theta}{2}\cos\frac{3\theta}{2}$$

where (r, θ) are the polar co-ordinates centred on the crack tip with the direction of crack growth being $\theta=0$. Additional terms can be added to these equations to account for mode II and III displacements, which in the case of the x-direction components of stress are:

$$\sigma_x = \frac{-K_{II}}{\sqrt{2\pi r}}\sin\frac{\theta}{2}\left(2-\cos\frac{\theta}{2}\cos\frac{3\theta}{2}\right)$$
$$\tau_{xz} = \frac{-K_{III}}{\sqrt{2\pi r}}\sin\frac{\theta}{2} \quad (2)$$

There are corresponding expressions for the y-direction components of stress that are omitted here in the interests of brevity. The assumption of pure mode I displacements allows only Eq. 1 to be considered so that the only unknown K_I, can be solved using data from a measurement at a single point.

A better representation of the stress field is obtained by taking measurements along a selected line, such as $\theta=\pi/2$, which allows mode II displacements to be considered. Such methods have been developed for photoelasticity [5], moiré interferometry [6] and thermoelasticity [7].

Finally, the most sophisticated approach is to use the full form of the stress field equations and to fit the three-dimensional surface that they describe in the stress-space (σ-x-y) domain to the one defined by a large number of measurements. Sanford and Dally [8] pioneered this method, known as the multi-point over-deterministic method (MPODM), in photoelasticity and variants have been developed for caustics [9], moiré interferometry [10], and thermoelasticity [11].

Thermoelasticity

When a body is subject to cyclic elastic stresses, it experiences a cyclic variation in temperature that is out-of-phase with the variation in stress. These temperature changes can be measured with a sensitive infrared detector and the signal from the detector is proportional to the sum of the principal stresses. The thermoelastic effect is a reversible conversion between mechanical and thermal energy, since the temperature excursion will revert when the load is withdrawn. However, this energy conversion is only reversible if the elastic range of the material is not exceeded and there is no significant

heat transport during the loading and unloading. If reversible conditions are achieved and the frequency is high enough to ensure adiabatic conditions, the temperature changes can be related to the sum of principal stresses according to the following expression:

$$\Delta T = -\frac{\alpha T}{\rho C_p}\Delta(\sigma_1 + \sigma_2) \tag{3}$$

Where ΔT is the temperature variation due to the thermoelastic effect, α is the coefficient of thermal expansion, T is the absolute temperature of the material, ρ is the density, C_p is the specific heat at constant pressure and σ_1 and σ_2 are principal stresses.

The common practice in thermoelasticity is to measure ΔT by differential infrared thermal cameras, whose sensitivity and resolution are suitable for the very small the temperature changes induced by the thermoelastic effect (just a few mK). The principle of these cameras is based on the detection of the changes in radiant photon emittance induced by the changes in temperature. Consequently, the thermal signal obtained is proportional to the thermal emittance from the specimen surface and can be directly related to the sum of principal stresses according to the following expression:

$$\Delta(\sigma_1 + \sigma_2) = AS \tag{4}$$

when the coefficient of thermal expansion and the modulus of elasticity are independent of temperature, where A is the calibration constant and S is the thermoelastic signal. The calibration constant depends on the material being tested and the sensor properties.

Stanley and Chan [7] proposed a method for determining stress intensity factors using data obtained from a raster scan of a component by a single detector. Substitution for any point (r, θ) of Westergaard's equations (Eqs. 1 and 2) into Eq. 4 leads to:

$$AS = \frac{2K_I}{\sqrt{2\pi}}\cos\left(\frac{\theta}{2}\right) - \frac{2K_{II}}{\sqrt{2\pi}}\sin\left(\frac{\theta}{2}\right) \tag{5}$$

For the case of a pure mode I crack, $K_{II}=0$ and letting $y=r\sin\theta$ Eq. 5 becomes:

$$AS = \frac{2K_I}{\sqrt{2\pi}}\sqrt{\sin\theta}\cos\left(\frac{\theta}{2}\right) \tag{6}$$

Along a line parallel to the crack (y=constant) the maximum signal, S_{max} occurs when $\theta = \pi/3$, hence

$$y = \left(\frac{3\sqrt{3}K_I^2}{4\pi A^2}\right)\frac{1}{S_{\max}^2} \tag{7}$$

In practice S is plotted against x for a large number of y values in order to obtain S_{max}. The stress intensity factor is then obtained from the gradient of a graph of y against $1/S_{max}^2$ using the following expression:

$$\Delta K_I = \sqrt{\frac{4\pi A^2}{3\sqrt{3}} \frac{d\left(S_{\max}^{-2}\right)}{dy}} \tag{8}$$

A similar procedure can be followed for pure mode II cracks except that $K_I=0$ in Eq. 5. Mixed mode loading is a little more complicated since a series of parallel plots of the signal are required on each side of the crack. For each side of the crack a plot of y against $1/S_{max}^2$ is produced and the pair of gradients is used to solve simultaneous equations in K_I and K_{II}. This method was used by Pang [12] to study interacting coplanar part-through cracks and by Leaity and Smith [13] to examine the relationship between measured, applied and effective ΔK.

In 1993 Stanley and Dulieu-Smith [14] evaluated the method for determining mixed mode stress intensity factors and concluded that the accuracy was moderate and the repeatability was poor. In the same paper, Stanley and Dulieu Smith developed another procedure based on the fact that isopachic contours in the crack tip region normally take the shape of a cardioid curve. By studying the orientation and shape of the cardioid they were able to estimate the SIF directly from thermoelastic data. Lesniak [15] also developed a method that operated by fitting a mathematical model based on Airy's functions to a set of thermoelastic data collected from a region surrounding the crack tip using a non-linear least squares method. Lin *et al*. [16] developed a methodology for the SIF calculation on composites materials based on a J-integral approach.

Tomlinson *et al.* [17] adapted the MPODM based on Muskhelishvili's approach from photoelasticity to thermoelasticity and achieved a better level of accuracy than had been observed using earlier methods. For this method, Eq. 6 can be re-written as

$$h_i = 2\Delta\left(\phi(\varsigma) + \overline{\phi(\varsigma)}\right) - AS \tag{9}$$

which was solved using a Newton-Raphson iterative method.

In all the previous methodologies the crack tip was either not considered in the SIF calculation, such is the case of Stanley and Chan's approach, or it had to be introduced manually. This constitutes a major source of error and uncertainty since data close to the crack tip are blurred due to the lack of adiabatic conditions. There are two phenomena that lead to the lack of adiabaticity near the crack tip region, one is the heat generation due to plastic work and the other is the presence of high stress gradients. In these conditions the direct observation of the crack tip from thermoelastic data becomes difficult. Nevertheless, work has been conducted trying to develop a methodology for the crack tip location based on the phase map [18, 19].

A new algorithm [19, 20], based on the work of Tomlinson *et al*. [17], has been developed to include the crack tip position in the K-calculation. The procedure is to fit

the experimental thermoelastic data collected at the crack tip region to a mathematical expression describing the distribution of the sum of principal stresses at the crack tip. The mathematical model is based on Muskhelishvili's approach [21], where the in-plane stresses are described by two analytical functions of a complex variable. Moreover, the stress equations are expressed as Fourier series in complex form where the coefficients of each term are complex variables that allow different states to be modelled. An initial estimation for the crack tip location is required to start the calculation of the SIF from thermoelastic images. This initial estimate is taken from the phase information of the thermoelastic data. The algorithm then searches for the crack tip location that minimizes the error for the fitting expression. The numerical method employed in the optimisation process is based on the Down-Hill Simplex method. This numerical approach is more robust than other methods since it is not based on the derivative of an error function.

This new methodology makes it possible to include the crack tip location as a variable to be optimised into the fitting process. As a result, the crack tip location obtained from each processed image can be employed to monitor the fatigue crack path.

APPLICATION OF TSA TO A FATIGUE CRACK IN A WELD

In thermoelasticity, the fact that the crack tip stresses are derived from the thermal response of the specimen due to cyclic loading means that it is the effective stress intensity factor range that is derived. In principle, therefore, one should be able to measure crack closure using TSA. An experimental programme was set up to test this hypothesis and also to determine whether the new computer algorithm developed for the SIF calculation could be employed as a tool to monitor the fatigue crack path from the calculated crack tip coordinates.

For the experiments reported in this paper a Deltatherm 1550 system from Stress Photonics Inc. was employed. This is based around an In-Sb infrared starring array detector that makes possible to collect data simultaneously from 320 by 256 pixels window. The digital signal processing considerably reduces the data acquisition time to just a few seconds, ensuring that during the data collection period the crack does not grow. Moreover, this system makes it possible to achieve a maximum spatial resolution of 25 μm.

The test specimens were manufactured from two BS 1501 490 LT50 ferritic steel plates welded together along their edges. The welding was performed by a multipass submerged arc process using an asymmetric double V preparation. The welded plate was then rewelded to simulate the site repair of a central root defect in the original weld. This involved grinding out from the narrower side of the weld to a depth of 17 mm and rewelding with a lower heat input. Neither the original weld nor the repair weld were subjected to any post-weld heat treatment. The mechanical properties of the steel and a complete description of the specimen manufacture are detailed in reference [22]. The fatigue specimens for the repair welds were single edge notched tensile bars with the weld in the central part and a 4 mm spark eroded notch in the deeper side of the weld, as

shown in Fig. 1. One specimen was heat treated after manufacture to minimise the welding residual stresses.

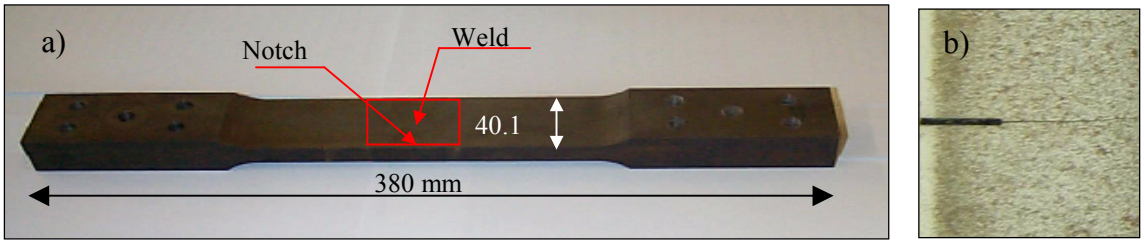

Figure 1. a) Test specimen. b) Detail of the notch.

The specimens were prepared by spraying the front surface with a matt-black paint (RS type 496-782) to increase the surface emissivity. Two rosette strain gauges (Tokyo Sokki Kenkyujo Co., 2 mm, 120 ± 0.5 Ω) were bonded on the rear face for calibration purposes. One was at the crack line and the other one far away from the crack to avoid the influence of high stress gradients.

Test specimens were installed in an ESH servohydraulic machine with a maximum load range of 100 kN using an assembly consisting of two grips and two pins to ensure pure axial loading. Constant amplitude tensile loads were applied along the longitudinal axis at a frequency of 12 Hz. Fatigue experiments were conducted at R-ratios from 0.1 to 0.6.

During the different fatigue tests performed, thermoelastic images were captured whilst the fatigue cracks grew. An example of the images is shown in Fig. 2. Simultaneously, the crack length was monitored from the rear side of the specimen using a vernier microscope. Finally, thermoelastic images were processed to locate the crack tip and evaluate the mode I and mode II stress intensity factor ranges.

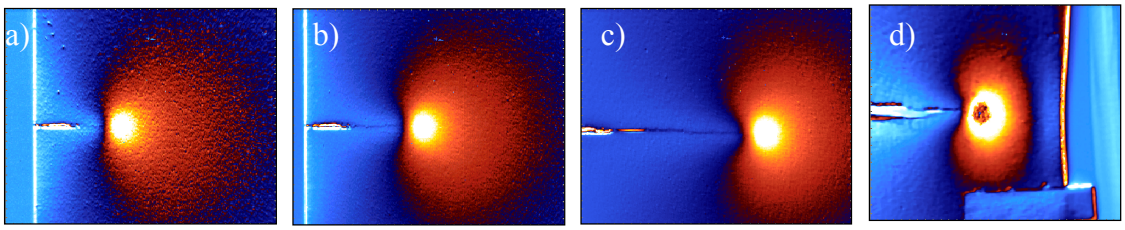

Figure 2. Thermoelastic images captured during a fatigue test, a) 311,520 cycles (crack length 6.1 mm), b) 413,320 cycles (8.0 mm), c) 506,327 cycles (17.4 mm) and d) 534,140 cycles (32.9 mm).

DISCUSSION OF THE RESULTS

The stress intensity factors determined experimentally are plotted against crack length in Fig. 3 for the stress relieved and repair welded specimens, both tested at a load ratio of 0.1. The continuous line represents the mode I SIF range calculated from the applied load range [23], while the points correspond to the mode I SIF range obtained using TSA. Mode II data are not presented here since, as in previous work [18-20], the ΔK_{II} values inferred from TSA data were almost zero because the tests were set up to be under pure mode I conditions.

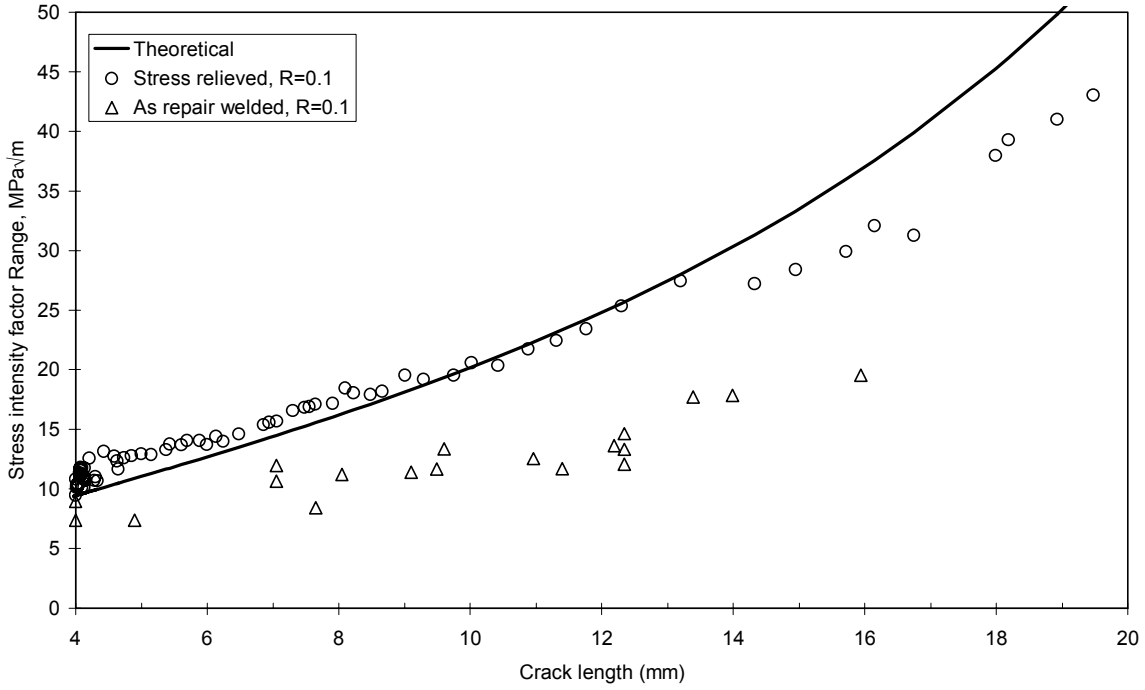

Figure 3. Comparison of mode I stress intensity factor range versus crack length data for repair welded and stress relieved specimens using TSA.

It is clear that the the TSA technique is picking up the effective stress intensity factor range of the growing crack by the substantial difference between the stress relieved and repair welded specimens. The repair welded specimen contains large tensile residual stresses over the first 10 mm of the specimen, changing to large compressive stresses from 10 mm through the centre of the plate [22]. This combined with the load R ratio means that the effective stress intensity factor range would be expected to be much lower than the theoretical value.

The effective stress intensity factor range of the stress relieved specimen deviates slightly from the expected values beyond a length of 14 mm. It is not clear whether this is a closure effect or a shortcoming in the stress intensity calibration for this geometry.

In Fig. 4 are shown the data for the repair welded specimens tested over a range of load ratios. Again, the ability of the TSA technique to measure effective stress intensity factor ranges is clearly shown. A reduction in closure is apparent as the mean load is increased. However, even at R=0.6 the experimental data deviate from the expected values at crack lengths beyond 14 mm.

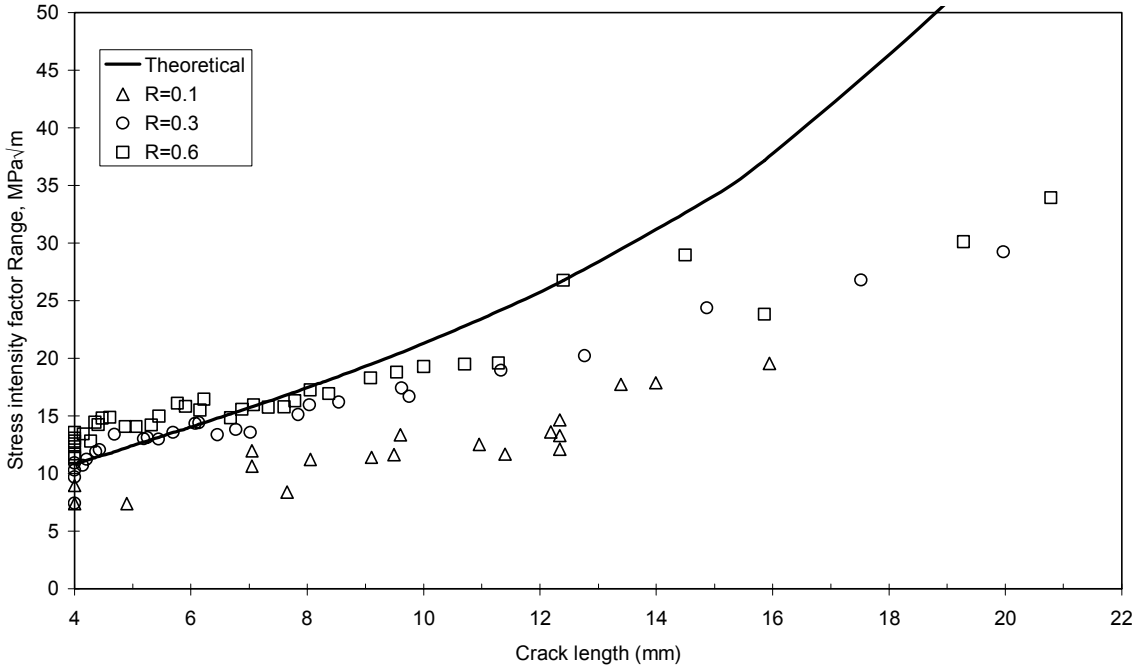

Figure 4. Influence of mean load on mode I stress intensity factor ranges versus crack length results for repair welded specimens using TSA.

The result of locating the crack tip in the thermoelastic images is shown in Fig. 5. The precision of the technique can be clearly seen. The ease and accuracy with which the crack tip can be located means that TSA has great potential in the study of crack growth in complex structures with complex stress fields.

The ability to locate the crack tip automatically makes the measurement of the fatigue crack growth rate much easier. Growth data for the repair weld is plotted against the effective stress intensity factor range in Fig. 6.

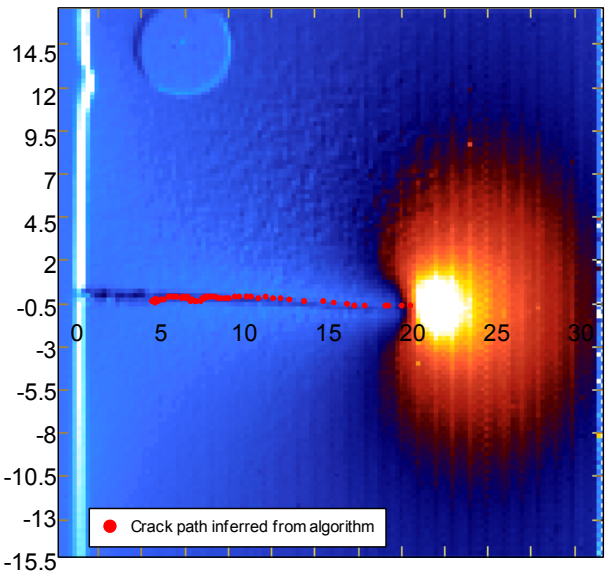

Figure 5. Fatigue crack path inferred by processing thermoelastic images captured during a fatigue test performed at R = 0.1

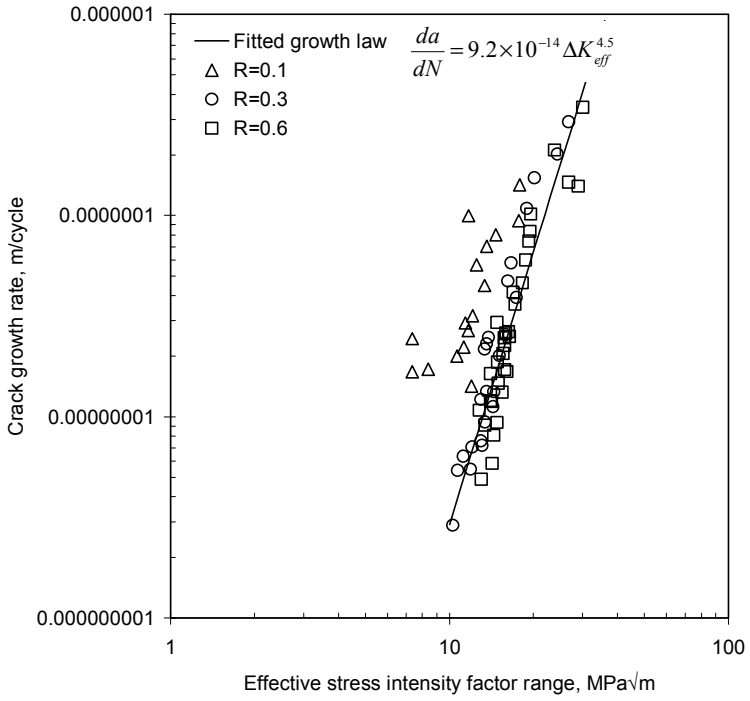

Figure 6. Fatigue crack growth rate against the effective ΔK range for fatigue tests conducted at different R-ratios using TSA.

CONCLUSIONS

In the present paper, thermoelastic stress analysis has been presented as technique with an enormous potential in the study of different fatigue crack growth mechanisms. The technique has been successfully employed in the experimental evaluation of the fatigue crack path from thermoelastic images. Moreover the technique seems to be sensitive to the crack closure mechanisms, since changes in the ΔK are observed when the R-ratio changes or when the specimen is stress relieved. However, more work is being conducted to validate the experimental results against conventional compliance methods.

ACKNOWLEDGEMENTS

Some of this work was undertaken as part of a collaborative project with AEA Technology, now Serco Assurance, and M R Goldthorpe and Associates for the Health and Safety Executive. Their assistance is gratefully acknowledged. Other parts of this work were supported by an EPSRC grant (GR/M57712/01) for which the authors are also grateful. Dr. Mark Pacey and Prof. Neil James are also thanked.

REFERENCES

1. Sanford, D. J. (1989) *Exptl. Mech*., 241-247.
2. Patterson, E.A. and Olden, E.J. (2004) To appear in *Fatigue Fract. Engng Mater. Struct.* **27**.
3. Irwin, G.R. (1958) *Proc. Soc. Exp. Stress Anal*. **16**, 93-96.
4. Westergaard, H.M. (1939) *ASME Trans., J. Appl. Mech.,* A49-53.
5. Schoedl, M.A. and Smith, C.W. (1973) In: *ASTM STP 536*, 45-63.
6. Nicoletto, G., Post, D. and Smith, C.W. (1982) In: *Proc. SESA/JSME joint conference on Experimental Mechanics*, 266-270.
7. Stanley, P. and Chan, W.K. (1986) *Proc. IMechE*. **C262***,* 105-114.
8. Sanford, R. J. and Dally, J.W. (1979) *Engng. Fract. Mech*. **11,** 621-633.
9. Carazo-Alvarez, J.D. and Patterson, E.A. (1999) *Optics and Lasers in Engng.* **32**, 95-110.
10. Barker, D.B., Sanford, R.J. and Chona, R. (1985) *Exptl Mech*. **25**, 399-405.
11. Tomlinson, R.A., Nurse, A.D. and Patterson, E.A. (1997) *Fatigue Fract. Engng Struct.* **20**, 217-226.
12. Pang, H. L. J. (1993) *Exptl. Tech*. **17**, 20-22.
13. Leaity, G.P. and Smith R.A. (1989) *Fatigue Fract. Engng Mater. Struct.* **12**, 271-282.
14. Stanley, P. and Dulieu-Smith, J.M. (1993) In: *Proc. SEM Spring Conf. Exptl. Mech*., Dearborn, USA, 617-626.
15. Lesniak, J.R., Bazile, D.J., Boyce, B.R., Zickel, M.J., Cramer, K.E. and Welch, C.S. (1996) In: *Strain and Damage in Materials and Structures*, Orlando, USA, 271-282.

16. Lin, S.T., Feng, Z. and Rowlands, R.E. (1997) *Engng. Fract. Mech*. **56**, 579-592.
17. Tomlinson, R.A., Nurse, A.D. and Patterson, E.A. (1993) *Fatigue Fract. Engng Mater. Struct.* **20**, 217-226.
18. Díaz, F.A., Tomlinson, R.A., Yates, J.R. and Patterson, E.A. (2002) In: *Proc. 2002 SEM Annual Conf.*, Milwaukee, USA, Paper 98.
19. Díaz, F.A., Yates, J.R. and Patterson, E.A. (2004) To appear in *Int. J. Fatigue* **26**.
20. Díaz, F.A., Patterson, E.A. Tomlinson, R.A. and Yates, J.R. (2004) To appear in *Fatigue Fract. Engng Mater. Struct.* **27**.
21. Muskheslishvili, N.I. (1953) *Some basic problems of the Mathematical Theory of Elasticity*, P. Noordhoff Ltd., Groningen, Holland.
22. Sharples, J.K., Gardner, L., Bate, S.K., Charles, R., Yates J.R. and Goldthorpe, M.R. (2001) *Integrity of Repaired Welds (Phase 1),* Serco Assurance plc., Warrington, Cheshire, UK.
23. Murakami, Y. (1987) *Stress Intensity Factor Handbook*, Pergamon Press, Oxford.